
Since January 2020 Elsevier has created a COVID-19 resource centre with free information in English and Mandarin on the novel coronavirus COVID-19. The COVID-19 resource centre is hosted on Elsevier Connect, the company's public news and information website.

Virology 460-461 (2014) 180–193

Contents lists available at ScienceDirect

Virology

journal homepage: www.elsevier.com/locate/yviro

# Porcine epidemic diarrhea virus induces caspase-independent apoptosis through activation of mitochondrial apoptosis-inducing factor

Youngnam Kim, Changhee Lee *

*Animal Virology Laboratory, School of Life Sciences, BK21 Plus KNU Creative BioResearch Group, Kyungpook National University, Daegu 702-701, Republic of Korea*

ARTICLE INFO

*Article history:*
Received 25 March 2014
Returned to author for revisions
16 April 2014
Accepted 30 April 2014
Available online 5 June 2014

*Keywords:*
PEDV
Apoptotic cell death
Caspase-independent
Apoptosis-inducing factor
Pathogenesis

ABSTRACT

The present study sought to investigate whether porcine epidemic diarrhea virus (PEDV) induces apoptosis and to elucidate the mechanisms associated with apoptotic cell death after PEDV infection. PEDV-infected cells showed evidence of apoptosis *in vitro* and *in vivo*. However, experimental data indicated that the caspase cascade is not involved in PEDV-induced apoptotic cell death. Interestingly, mitochondrial apoptosis-inducing factor (AIF) was found to translocate to the nucleus during PEDV infection, and AIF relocalization was completely abrogated by the presence of cyclosporin A (CsA), an inhibitor of cyclophilin D (CypD) that is an essential component of the mitochondrial permeabilization transition pore (mPTP) complex. CsA treatment resulted in significant inhibition of PEDV-triggered apoptosis and suppressed PEDV replication. Furthermore, direct inhibition of AIF strongly impaired PEDV infection and virus-induced apoptosis. Altogether, our results indicate that a caspase-independent mitochondrial AIF-mediated pathway plays a central role in PEDV-induced apoptosis to facilitate viral replication and pathogenesis.



## Introduction

Porcine epidemic diarrhea (PED) is a devastating disease of swine that was initially recognized in the United Kingdom in 1971 and that has then spread to swine-producing European countries (Oldham, 1972; Pensaert et al., 1981). Since the 1990s, the disease has become rare in Europe and is more often associated with postweaning diarrhea in adult pigs (Saif et al., 2012). PED epidemics were first reported in Asia in 1982 and since then, PED has continued to threaten swine health causing substantial financial losses in the Asian swine industry (Chen et al., 2008; Kweon et al., 1993; Li et al., 2012; Puranaveja et al., 2009; Takahashi et al., 1983). In 2013, PED outbreaks suddenly appeared in the United States and have swept the national pork industry with high mortality in newborn piglets, posing significant economic and public health concerns (Mole, 2013; Stevenson et al., 2013). In 1978, the etiological agent of this disease was identified as a coronavirus, PED virus (PEDV), which belongs to the genus *Alphacoronavirus* within the family *Coronaviridae* of the order *Nidovirales* (Pensaert and de Bouck, 1978; Saif et al., 2012). PEDV is a large, enveloped virus possessing a single-stranded positive-sense RNA genome of approximately 28 kb with a 5′ cap and a 3′ polyadenylated tail (Pensaert and de Bouck, 1978; Saif et al., 2012). The PEDV genome is composed of a 5′ untranslated region (UTR), at least 7 open reading frames (ORF1a, ORF1b, and ORF2 through 6), and a 3′ UTR (Kocherhans et al., 2001). The two large ORF1a and 1b cover the 5′ two-thirds of the genome and encode the non-structural replicase genes. The remaining ORFs in the 3′ terminal region code for four major structural proteins, the 150–220 kDa glycosylated spike (S) protein, 20–30 kDa membrane (M) protein, 7 kDa envelop (E) protein, and 58 kDa nucleocapsid (N) protein (Duarte et al., 1994; Saif et al., 2012).

PEDV is a pathogenic enterocyte-tropic coronavirus of swine, and its infection is marked by acute enteritis with mortality approaching 100% in suckling piglets up to one week of age (Debouck and Pensaert, 1980; Saif et al., 2012). The virus is transmitted via the fecal-oral route and the virus replicates in the cytoplasm of villous epithelial cells throughout the small intestine. PEDV infection results in severe villous atrophy, leading to a reduction in the villous height:crypt depth ratio from the normal 7:1 to 3:1. This interrupts digestion and absorption of nutrients and electrolytes, thereby causing malabsorptive watery diarrhea followed by serious and fatal dehydration in piglets (Saif et al., 2012). In addition, PEDV can be propagated in Vero (African green monkey kidney) cells *in vitro*, where the cytopathic effects

* Correspondence to.: School of Life Sciences, College of Natural Sciences, Kyungpook National University, Daegu 702-701, Republic of Korea.
Tel.: +82 53 950 7365; fax: +82 53 955 5522.
*E-mail address:* changhee@knu.ac.kr (C. Lee).

http://dx.doi.org/10.1016/j.virol.2014.04.040
0042-6822/

(CPEs) consist of vacuolation and formation of syncytia with up to 100 nuclei (Hofmann and Wyler, 1988). However, the mechanisms inducing cell death in PEDV-infected target cells, both *in vitro* and *in vivo*, remain poorly understood.

Apoptosis is a tightly regulated mechanism of cell death that is triggered by various extracellular (extrinsic) or intracellular (intrinsic) stimuli and modulated by anti- and pro-apoptotic cellular factors (Galluzzi et al., 2012). Cells undergoing apoptosis are accompanied by characteristic morphological changes, including rounding-up of the cell, chromatin condensation, nuclear fragmentation, and plasma membrane blebbing (Kroemer et al., 2009). Apoptosis is considered to be a host innate defense mechanism that disrupts viral replication by eliminating virus-infected cells. Therefore, viruses have developed strategies to avoid apoptosis, which, in turn, prevent premature cell death and thus maximize progeny viral production (Thomson, 2001). However, many viruses have the ability to actively induce apoptosis as a response to viral replication, thereby facilitating the release and dissemination of viral progeny to neighboring cells. This pro-apoptotic event is one of the cytolytic properties of viral infections causing CPE *in vitro* or/and plays a pathogenic role contributing to cell damage, tissue injury, and disease severity *in vivo* (Clarke et al., 2009; Clarke and Tyler, 2009; DeDiego et al., 2011; Eleouet et al., 1998; Favreau et al., 2012; Lan et al., 2013; Lee and Kleiboeker, 2007; St-Louis and Archambault, 2007; Sarmento et al., 2006; Suzuki et al., 2008). At present, it is unknown whether PEDV triggers apoptotic cell death, and if so, whether virus-induced apoptosis aids or worsens viral replication and pathogenicity. Therefore, in this study, we aimed to determine if PEDV induces apoptosis following infection *in vitro* and *in vivo* and to define the specific pathways involved in apoptotic death of virus-infected cells. Apoptotic cell death occurred after *in vitro* and *in vivo* infections of PEDV, suggesting that PEDV-induced apoptosis may play an important role in cytotoxicity and pathogenesis. Treatment with a pan-caspase inhibitor failed to suppress PEDV-induced apoptosis and PEDV infection. However, PEDV replication and virus-triggered apoptosis were significantly impaired by inhibitors of cyclophilin D (CypD) and apoptosis-inducing factor (AIF). These data indicate that PEDV promotes AIF-mediated and caspase-independent apoptosis, which is essential for the replication of PEDV. Overall, our study will improve the understanding of the correlation between PEDV-induced apoptosis and its pathogenic mechanisms and show the potential of anti-apoptotic therapeutic strategies for combating PEDV infection.

## Results

### *PEDV induces programmed cell death in vitro and in vivo*

To investigate whether apoptotic cell death was triggered by PEDV, virus-infected cells were first examined for the presence of DNA fragmentation, which is a hallmark of cells undergoing apoptosis. Vero cells were infected with PEDV, and CPE was monitored after infection. Light microscopy of the PEDV-infected Vero cells indicated that typical CPEs characterized by vacuolation and syncytia formation were visible starting at 24 hpi and became prominent by 48 hpi (Fig. 1A, upper panels). To detect intracellular fragmented DNA, cellular DNA from mock- or virus-infected cells was harvested and subjected to a DNA laddering assay. Consistent with the CPE observation results, intracellular DNA fragmentation appeared at 24 hpi, and the DNA ladder pattern was apparent at 48 hpi (Fig. 1A, lower panel). This characteristic of apoptosis was further confirmed using a TUNEL assay. As shown in Fig. 1B, compared to mock-infected cells, TUNEL-labeled cells were only observed within virus-infected cells. The process of PEDV-induced apoptosis was then assessed using Annexin V/PI flow cytometry. Virus- or mock-infected cells were stained with Annexin V and PI and then examined using FACS flow cytometry to quantitatively determine the percentage of viable, apoptotic, and dead cells. PEDV infection produced a high level of apoptosis (Annexin V positive/PI negative) appearing at 6 hpi, and the percentage of early apoptotic cells increased with infection time, reaching a maximum of 87.4% at 48 hpi (Fig. 1C). In addition, we sought to determine whether PEDV induces apoptosis in the natural host. To accomplish this, a TUNEL assay was performed to detect and quantify apoptosis in small intestine sections prepared from piglets experimentally inoculated with PEDV. Immunofluorescence using N protein-specific MAb revealed that abundant viral antigens were primarily present in enterocytes over the entire villi in all areas of the small intestine at 3 dpi and increasingly dominant in the interior of the villi at 5 dpi; the majority of virus-infected cells were TUNEL-positive (Fig. 2). In contrast, no TUNEL-positive enterocytes were observed in the tissue specimens prepared from a non-infected animal (Fig. S1). Taken together, these data demonstrate that PEDV infection induces apoptosis *in vitro* and *in vivo*.

### *Treatment with a pan-caspase inhibitor neither inhibits PEDV-induced apoptosis nor impairs PEDV infection*

Caspases, a family of aspartate-specific cysteine proteases, play critical roles in the execution phase of apoptosis of the cell leading to morphological and nuclear changes (Clarke and Tyler, 2009). In order to elucidate the mechanism and the type of apoptotic cell death, we initially assessed whether the broad-spectrum pan-caspase inhibitor, Z-VAD-FMK, blocks PEDV-induced apoptosis. Based on the results of the MTT assay, none of the doses of Z-VAD-FMK tested in the present study resulted in any change in cell viability (data not shown). Vero cells were treated with Z-VAD-FMK at concentrations of 100 μM followed by viral infection. At the indicated time points post-infection, virus-infected and Z-VAD-FMK-treated cells were analyzed based on FACS quantification of Annexin V binding. Notably, treatment with Z-VAD-FMK was incapable of protecting cells from PEDV-induced apoptosis (Fig. 3A). The percentage of early apoptotic cells in the presence of Z-VAD-FMK was almost similar to that in vehicle (DMSO)-treated cells (second panel) and PEDV-infected cells during the course of infection (compared to Fig. 1C). These results indicated that caspases are not associated with PEDV-triggered apoptosis. For further confirmation, we tried to determine the activity of caspase-3 upon PEDV infection by western blot analysis. Caspase-3 is the main executioner caspase activated by the both extrinsic and intrinsic apoptotic pathways causing the morphological features of apoptosis. As shown in Fig. 3B, no detectable level of cleaved caspase-3 was observed in PEDV-infected cells up to 48 hpi (first panel), whereas the N protein was first detected at 6 hpi, and its production greatly increased thereafter, indicating PEDV replication (third panel). On prolonged exposure of the western blot, however, it was apparent that a small amount of activated caspase-3 appears only at 48 hpi (second panel), which seems to be a basal level normally present at late time of infection. We next investigated if the replication of PEDV is also affected by the same caspase inhibitor. Vero cells were pretreated with Z-VAD-FMK at concentrations of 10–100 μM or with DMSO as a vehicle control for 1 h prior to infection. Z-VAD-FMK was present during the entire period of infection. Viral production was measured by monitoring CPE and confirmed by immunofluorescence at 48 hpi (Fig. 3C). Apparent CPE and N-specific staining were equally evident in cells treated with Z-VAD-FMK when compared to vehicle-treated control cells. Furthermore, PEDV replication, as quantified by the growth kinetics results, was not reduced by

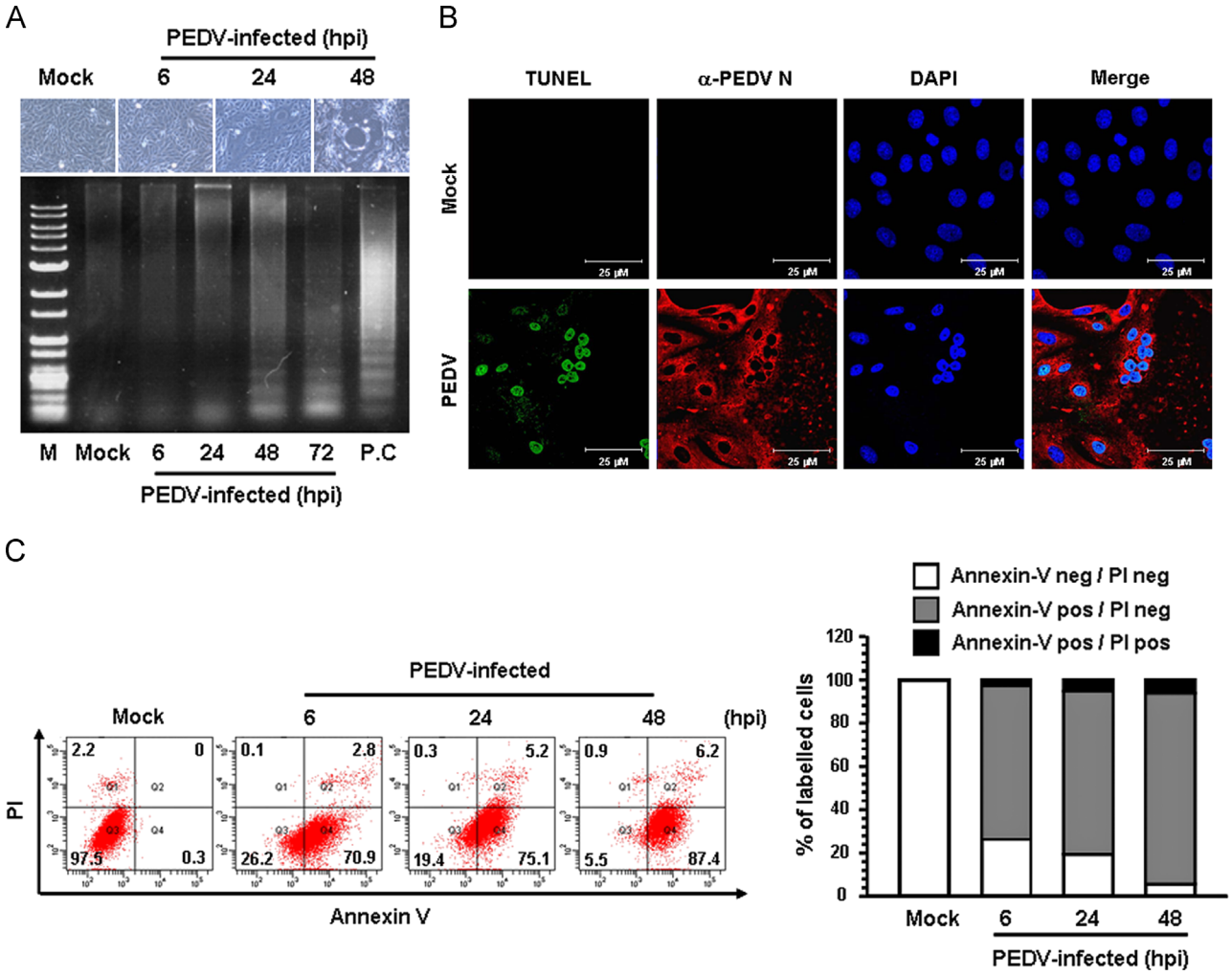


**Fig. 1.** PEDV infection induces apoptosis *in vitro*. (A) CPE observations and DNA fragmentation in PEDV-infected cells. Vero cells were mock-infected or infected with PEDV. At the indicated times post-infection, PEDV-specific CPEs were photographed using an inverted microscope at a magnification of 200 × (top panels). For the DNA fragmentation assay, DNA was extracted from mock- or PEDV-infected cells and nucleosomal DNA fragmentation of the cells was then analyzed by agarose gel electrophoresis (bottom panel). As a positive control, cells were treated with staurosporine for 24 h to induce apoptosis. Lane M represents a 1-kb ladder as a DNA molecular-weight size marker. (B) TUNEL labeling of PEDV-infected cells. Mock-infected control and PEDV-infected cells fixed at 48 hpi were labeled with TUNEL (green) and sequentially stained with an anti-PEDV-N antibody (red). The cells were then counterstained with DAPI and photomicrographs of TUNEL labeling and N protein staining in virus-infected cells was observed using a confocal microscope at 400 × magnification. In a merged image, all TUNEL-positive cells were localized within the nuclei of corresponding PEDV-infected cells. (C) Cell death analysis by flow cytometry with dual Annexin V-PI cell labeling. PEDV-infected cells collected from different time periods were dually labeled with Annexin V and PI and analyzed by FACS. The lower left quadrants represent intact cells (Annexin V negative/PI negative); the lower right quadrants represent early apoptotic cells (Annexin V positive/PI negative); the upper right quadrants indicate late apoptotic and/or necrotic cells (Annexin V positive/PI negative); the upper left quadrants indicate necrotic cells (Annexin V negative/PI positive). The figure is representative of three independent experiments. The graph on the right represents the percentage of each quadrant and the non-significant percentages of Annexin V-positive and PI-negative cells were excluded.

Z-VAD-FMK treatment, indicating that activation of caspases is irrelevant to PEDV replication (Fig. 3D). Altogether, our data reveal that caspase cascades are not activated by PEDV and their chemical inhibition diminished neither PEDV-induced apoptotic cell death nor viral replication, suggesting that caspase activation is dispensable for the process.

### *PEDV infection promotes AIF nuclear translocation but does not affect CytC relocalization*

Since caspases appear to be non-essential factors in PEDV-triggered apoptosis, we investigated an alternative caspase-independent apoptotic pathway mediated mainly by AIF in relation to apoptotic cell death induced by PEDV. AIF is a flavoprotein embedded in the outer surface of the mitochondrial inner membrane. Following apoptotic stimuli, AIF is proteolytically cleaved and truncated AIF is released from the mitochondria and translocates to the nucleus, where it causes high-molecular weight DNA fragmentation and chromatin condensation independently of caspases (Cregan et al., 2002; Daugas et al., 2000; Galluzzi et al., 2012; Joza et al., 2001; Lu et al., 2013; Yuste et al., 2005). Mitochondria plays a central role in the intrinsic apoptotic pathway by releasing proapoptotic factors, such as AIF and cytochrome *c* (CytC), through the mitochondrial permeability transition pore (mPTP), which is permeabilized in response to intracellular stress (Galluzzi et al., 2012). In order to study the potential role of mitochondrial AIF in the caspase-independent pathway of PEDV-induced apoptosis, thus, we first aimed to determine the subcellular localization of AIF in PEDV-infected cells using immunofluorescence confocal microscopy. Although AIF continued to localize broadly in the mitochondria after PEDV infection shown by its colocalization with a mitochondrial-specific marker, the majority of cells infected with PEDV also displayed a condensed AIF staining pattern within the nucleus, and its intensity was

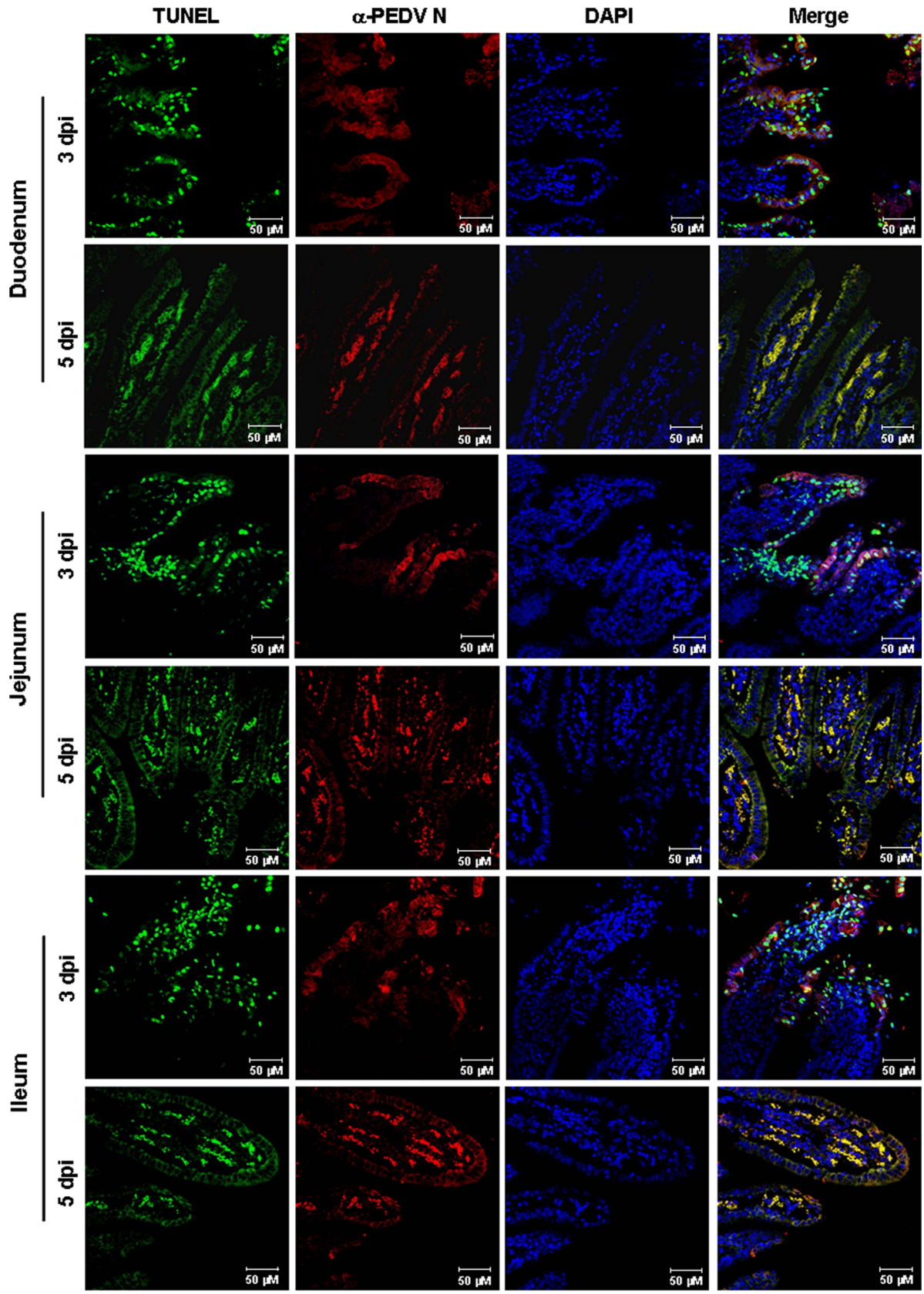


**Fig. 2.** PEDV infection induces apoptosis *in vivo*. Tissue specimens were collected from the duodenum, jejunum, and ileum of infected animals at the indicated days post-inoculation. The formalin-fixed and paraffin-embedded tissue sections were deparaffinized and sequentially labeled with TUNEL (green) followed by an anti-PEDV-N antibody (red). The sections were then counterstained with DAPI and examined using a confocal microscope at 200 × magnification. Yellow regions indicate merged images, where cells are positive for both TUNEL and PEDV infection.

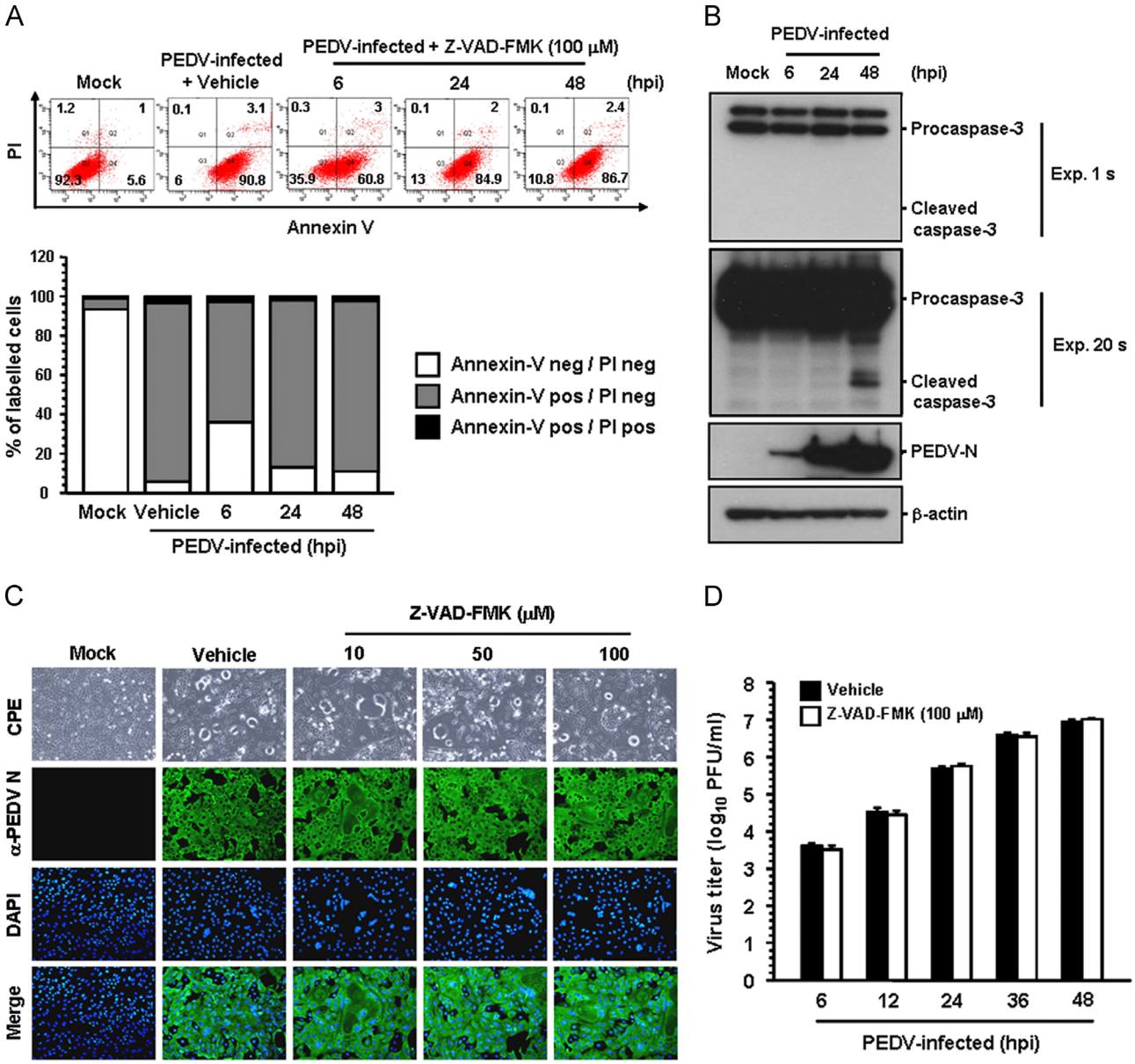


**Fig. 3.** Pan-caspase inhibitor does not affect PEDV-induced apoptosis and PEDV infection. (A) FACS with dual Annexin V-PI cell labeling in the presence of Z-VAD-FMK. Vero cells were pretreated with vehicle or Z-VAD-FMK (100 μM) for 1 h and were mock-infected or infected with PEDV in the presence of vehicle or Z-VAD-FMK. Cells were harvested at the indicated time points, dually labeled with Annexin V and PI, and subjected to FACS analysis. The bottom graph represents the percentage of each quadrant. (B) Western blot analysis of caspase-3. At the indicated time, the cellular lysates were collected, resolved by SDS-PAGE, transferred to a nitrocellulose membrane, and immunoblotted using an antibody that recognizes caspase-3 (top panel) or PEDV N protein (third panel). The second panel was imaged after longer exposure to confirm the presence of activated caspase-3. The blot was also reacted with mouse MAb against the β-actin gene to verify equal protein loading (bottom panel). The figures are representative of three independent experiments. (C) PEDV replication in the presence of Z-VAD-FMK. Vero cells were treated with Z-VAD-FMK at the indicated concentrations for 1 h prior to infection and were infected with PEDV. PEDV-infected cells were further maintained for 48 h in the presence of vehicle or Z-VAD-FMK. PEDV-specific CPEs were observed daily and were photographed at 48 hpi using an inverted microscope at a magnification of 200 × (first panels). For immunostaining, infected cells were fixed at 48 hpi and incubated with MAb against the PEDV N protein, followed by Alexa green-conjugated goat anti-mouse secondary antibody (second panels). The cells were then counterstained with DAPI (third panels) and examined using a fluorescent microscope at 200 × magnification. (D) Growth kinetics of PEDV in the presence of Z-VAD-FMK. At the indicated time points after infection, culture supernatants were harvested and viral titers were measured. Values are representative of the mean of three independent experiments and error bars represent standard deviations.

significantly elevated at 48 hpi (Fig. 4A, arrows). This observation was confirmed by western blot analysis of mitochondrial and nuclear extracts. As shown in Fig. 4B, an uncleaved 62 kDa AIF was detected in both extracts during the course of infection, whereas a cleaved form of AIF was observed only in nuclear extracts of PEDV-infected cells. We then analyzed the translocation of another proapoptotic protein, CytC, which is released to the cytoplasm by mitochondrial outer membrane permeabilization to execute caspase proteolytic cascade-dependent intrinsic apoptosis. In contrast to AIF, however, CytC was sustainedly located in the mitochondria of PEDV-infected cells, as demonstrated by the colocalization of CytC with MitoTracker and the detection of CytC in mitochondrial fractions (Fig. 4C and D). This CytC retention in the mitochondria during PEDV infection was concurrent with the caspase-independent apoptotic cell death induced by PEDV as described above. Consequently, our findings demonstrate that PEDV infection specifically triggers mitochondrial-nuclear translocation of AIF but not the release of mitochondrial CytC.

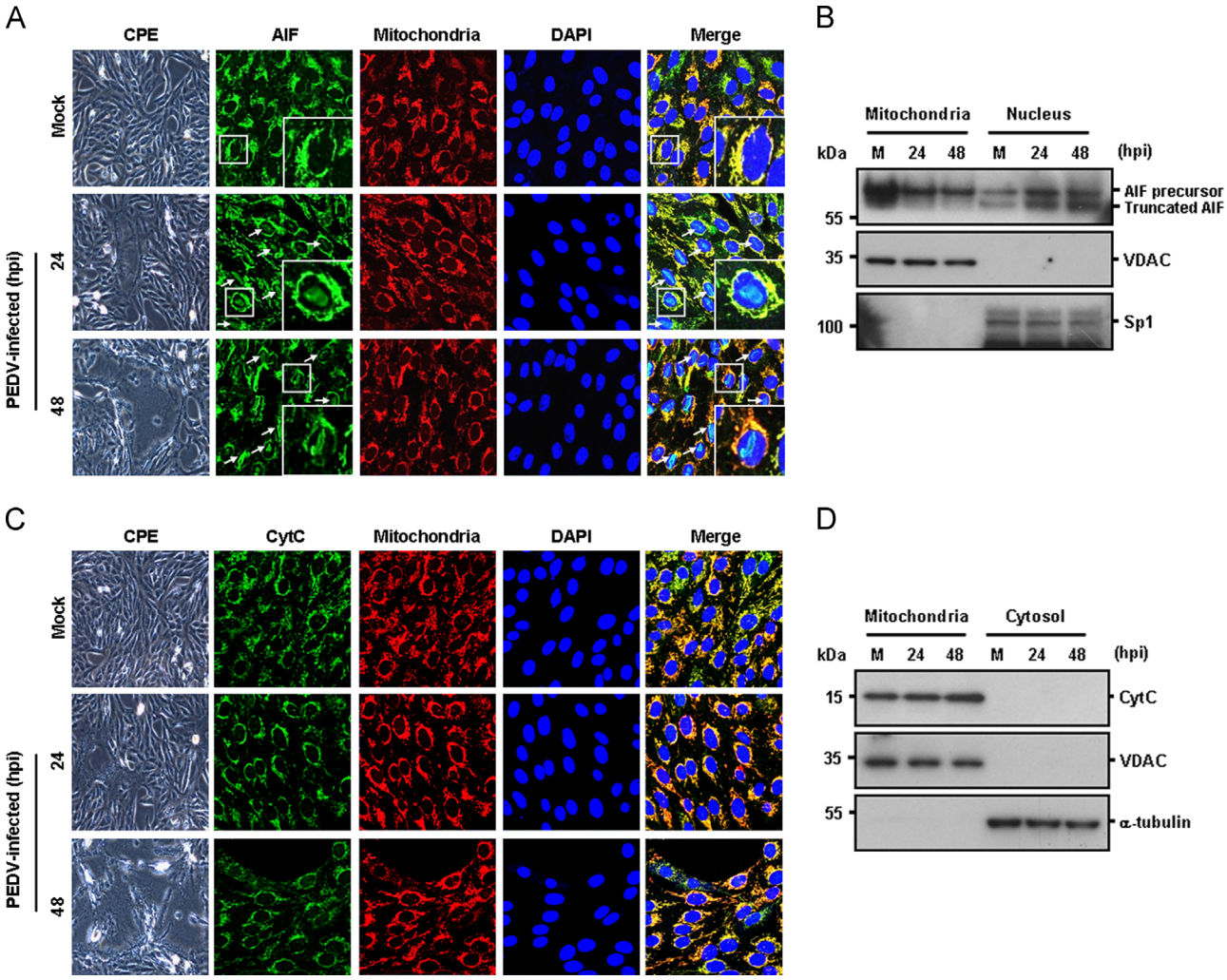


**Fig. 4.** PEDV infection promotes AIF translocation but not CytC release. (A) Immunofluorescent detection of AIF. At 24 hpi and 48 hpi, Vero cells mock-infected or infected with PEDV were labeled with MitoTracker Red CMXRos (red), fixed, and incubated with an anti-AIF antibody (green). AIF nuclear translocation is represented by merged AIF and DAPI signals (turquoise), indicated by white arrows, and residual mitochondrial colocalization is indicated by merged AIF and the mitochondrial marker (yellow). The inset images are enlarged versions of parts of the picture. (B) Western blot analysis of AIF. Each mitochondrial and nuclear fraction was prepared under the indicated conditions and subjected to western blotting with an antibody directed against AIF (top panel), VDAC as a mitochondrial protein marker (middle panel), or Sp1 as a nuclear protein marker (bottom panel). Lane M, mock-infected. (C) Immunofluorescent detection of CytC. PEDV-infected cells were incubated with MitoTracker Red CMXRos (red), fixed, and stained with an anti-CytC antibody (green). The mitochondrial accumulation of CytC is indicated by merged CytC and MitoTracker signals (yellow). (D) Western blot analysis of CytC. Each mitochondrial and cytosolic fraction was prepared under the indicated conditions and subjected to western blotting with an antibody against CytC (top panel), VDAC as a mitochondrial protein marker (middle panel), or α-tubulin as a cytosolic protein marker (bottom panel). Lane M, mock-infected. All subcellular protein markers also served as loading controls.

*Inhibition of cyclophilin D blocks PEDV-induced apoptosis and PEDV replication*

Cyclophilin D (CypD) is localized to the mitochondrial membrane matrix and is a main component in the process of mPTP opening (Baines et al., 2005; Schinzel et al., 2005). Therefore, we aimed to determine whether inhibition of CypD could prevent apoptotic cell death induced by PEDV. Cells were treated with CsA, a chemical inhibitor of CypD, to inhibit mPTP formation upon PEDV infection. The DNA laddering assay indicated that the presence of CsA in cells infected with PEDV completely abolished intracellular DNA fragmentation (Fig. 5A, lane 4), while cells infected with PEDV alone or combined with Z-VAD-FMK clearly displayed a DNA laddering pattern (Fig. 5A, lanes 2 and 3). Upon CsA treatment, PEDV-induced apoptosis was then quantitatively evaluated by Annexin V/PI flow cytometry. As shown in Fig. 5B, treatment with CsA notably decreased the percentage of early apoptotic cells induced by PEDV (second panel), ranging from 19.1% to 29.9% during the course of PEDV infection (compared to Fig. 3A). These results demonstrate that inhibition of CypD efficiently suppresses apoptotic cell death induced by PEDV, indicating that PEDV infection triggers the mitochondrial apoptotic pathway.

To examine the effect of CsA on PEDV replication, cells were pretreated with CsA at concentrations of 1–10 μM, and CsA was present during the entire period of infection. PEDV replication was determined by monitoring virus-specific CPE and verified by immunofluorescence at 48 hpi (Fig. 6A). In contrast to vehicle-treated control cells, CsA had a strong inhibitory effect on PEDV propagation by dramatically decreasing virus-induced CPE and viral gene expression even at the lowest concentration used. The number of cells expressing viral antigen, as quantified by N protein staining results, was also reduced during CsA treatment, resulting in almost complete inhibition in response to 10 μM (Fig. 6B). To further assess the antiviral activity of CsA against PEDV replication, viral yield was determined during treatment with CsA. Upon infection, viral supernatants were collected at 48 hpi, and viral titers were measured. As Fig. 6C shows, the presence of CsA

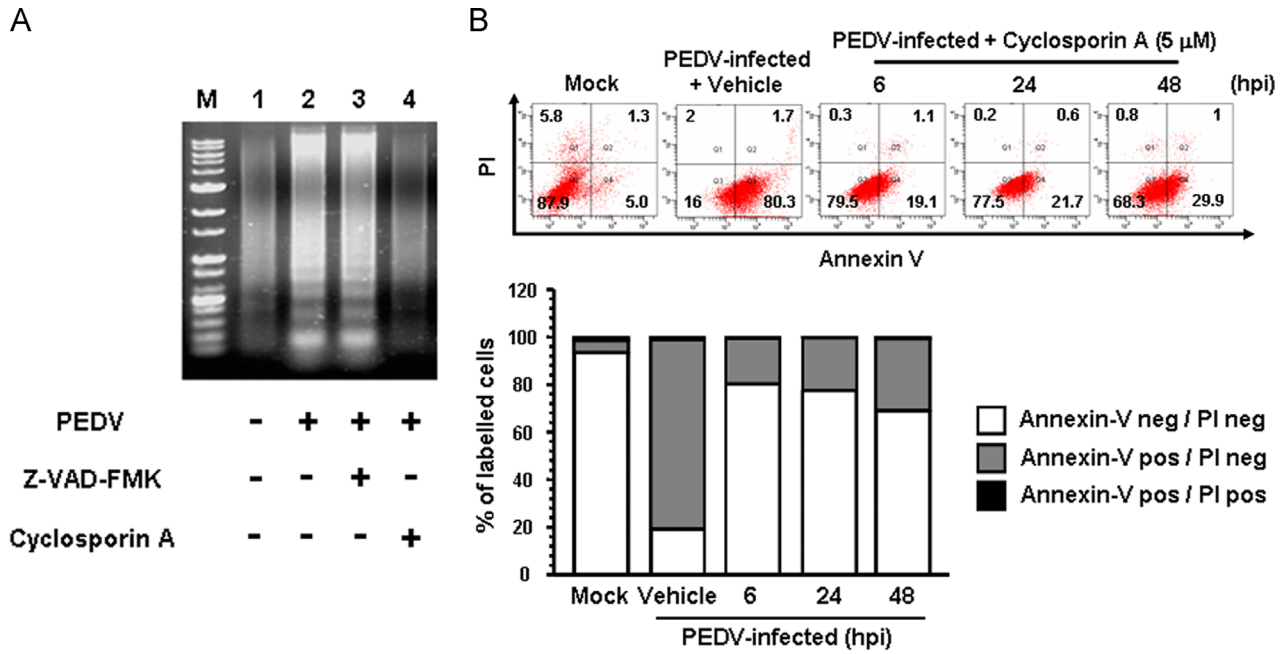


**Fig. 5.** CsA treatment abrogates PEDV-induced apoptosis. (A) DNA fragmentation analysis in the presence of CsA. Vero cells were preincubated with Z-VAD-FMK (100 μM) or CsA (5 μM) for 1 h and were mock-infected or infected with PEDV. Nucleosomal DNA fragmentation of the cells was analyzed by agarose gel electrophoresis. Lane M, DNA molecular-weight marker; lane 1, mock-infected and non-treated; lane 2, only PEDV-infected; lane 3, PEDV-infected and Z-VAD-FMK-treated; lane 4, PEDV-infected and CsA-treated. (B) FACS with dual Annexin V-PI cell labeling in the presence of CsA. Vero cells were pretreated with DMSO or CsA (5 μM) for 1 h and then mock-infected or infected with PEDV in the presence of vehicle or CsA. Cells were harvested at the indicated time points, dually labeled with Annexin V and PI, and subjected to FACS analysis. The bottom graph represents the percentage of each quadrant.

significantly reduced the release of viral progeny in a dose-dependent manner. The peak viral titer was determined to be $10^{6.68}$ PFU/ml in the vehicle-treated control, whereas the addition of 10 μM CsA declined the titer of PEDV to $10^{1.69}$ PFU/ml (an almost 5-log reduction compared to the control). The growth kinetics study further demonstrated that the overall process of PEDV replication was significantly delayed when cells were treated with CsA (Fig. 6D). In addition, we investigated whether viral protein translation and viral RNA synthesis were affected by CsA. The expression level of the PEDV N protein in the presence or absence of CsA was evaluated at 48 hpi by western blot analysis. Densitometric analysis of the western blot revealed that intracellular expression of the viral protein was entirely prevented by CsA at a concentration of 10 μM (Fig. 7A). Similarly, levels of both genomic RNA and sg mRNA were greatly diminished in a dose-dependent manner and their synthesis was fully abolished at the highest CsA concentration (Fig. 7B). Taken together, our data strongly indicate that CsA proficiently suppresses the replication of PEDV, which is correlated with inhibition of PEDV-induced apoptosis by CsA.

*Inhibition of cyclophilin D alters AIF nuclear translocation*

The present study shows that mitochondrial AIF is translocated to the nucleus following PEDV infection. Because CypD is involved in alteration of mitochondrial membrane permeability, followed by release of proapoptotic factors, it is conceivable that inhibition of CypD would block AIF nuclear translocation induced by PEDV, leading to impaired PEDV-induced apoptosis and viral replication. We therefore determined whether CsA specifically affects the nuclear translocation of AIF mediated by PEDV infection. Immunofluorescence confocal microscopy results demonstrated that AIF nuclear translocation in PEDV-infected cells was distinctly hampered following CypD inhibition by CsA, exhibiting a cytoplasmic distribution that colocalized with the mitochondrial marker during the entire course of PEDV infection (Fig. 8A). Mitochondrial retention of AIF in the presence of CsA was confirmed by a cell fractionation assay. As expected, the level of truncated AIF in the nuclear fractions was barely detectable in the presence of CsA, demonstrating that inhibition of CypD failed to cause the relocalization of AIF from the mitochondria to the nucleus (Fig. 8B). Altogether, these results suggest that upon PEDV infection, CypD-dependent mPTP directly modulates apoptotic cell death by relocating AIF to the nucleus, resulting in successful viral replication.

*AIF is involved in PEDV-induced apoptosis to promote viral replication*

Considering that AIF is a key proapoptotic protein released from the mitochondria in response to PEDV infection to trigger apoptosis, we sought to determine whether chemical inhibition of AIF could control PEDV-induced apoptosis and viral replication. To accomplish this, we first used an AIF inhibitor, *N*-PhMI, that prevents AIF-induced DNA fragmentation (Susin et al., 1996; Wang et al., 2007). Treatment with *N*-PhMI resulted in substantial reduction of the percentage of apoptotic cells during PEDV infection (Fig. 9). Addition of *N*-PhMI retained an average cell viability of over 80% during the entire time of PEDV infection, demonstrating that inhibition of AIF robustly represses apoptosis induced by PEDV. To further confirm the importance of AIF in apoptosis triggered by PEDV infection, we examined whether this drug alters the nuclear relocalization of AIF following PEDV infection by confocal microscopy analysis. As depicted in Fig. 10A, *N*-PhMI treatment completely abrogated AIF nuclear translocation induced by PEDV, leading to mitochondrial accumulation of AIF. Western blot analysis provided further support by showing the absence of truncated AIF in the nuclear fractions of PEDV-infected cells in the presence of *N*-PhMI (Fig. 10B). These results strongly indicated that nuclear targeting of AIF is required for PEDV-induced apoptotic cell death.

Finally, to determine whether AIF function is necessary for PEDV replication, Vero cells were treated with *N*-PhMI for 1 h prior

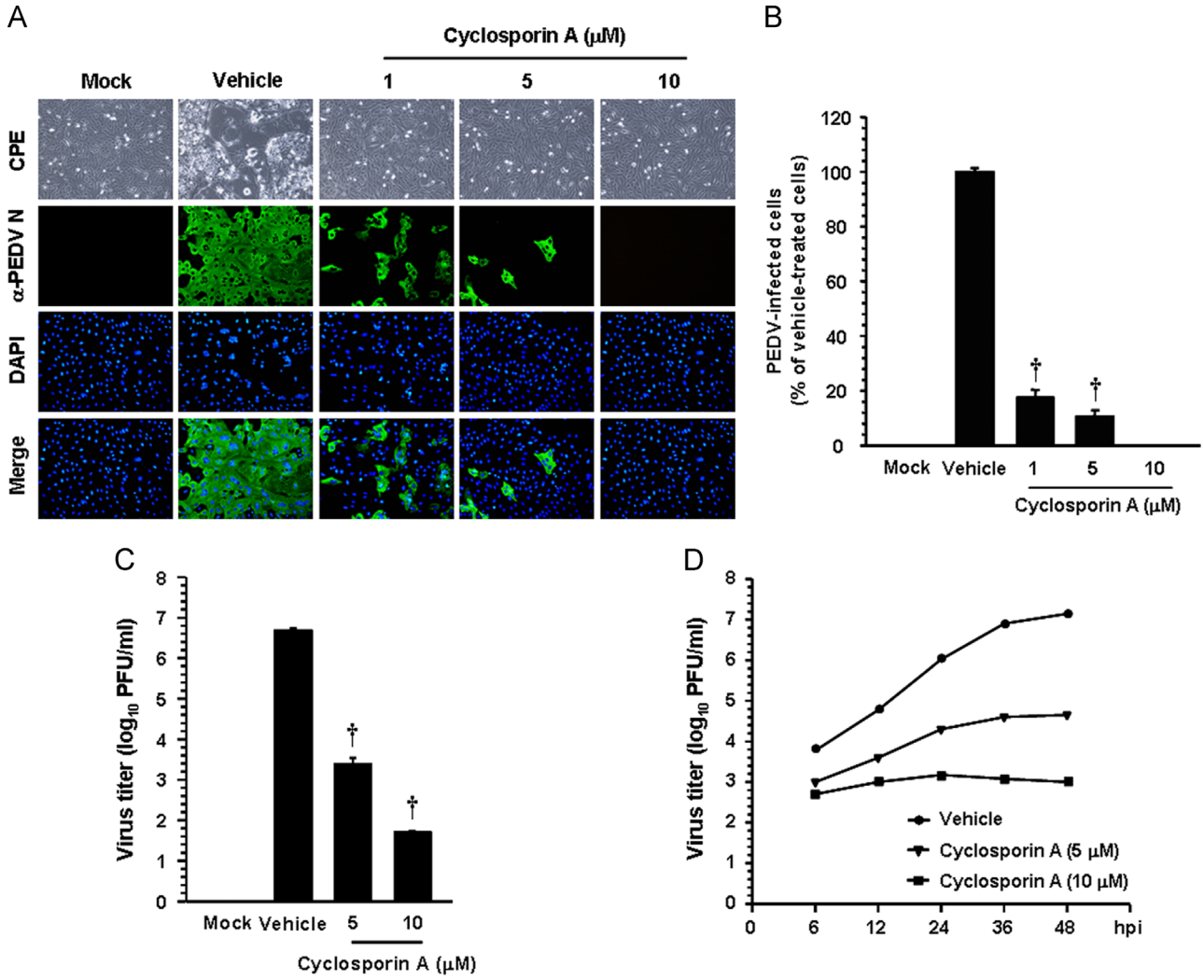


**Fig. 6.** CsA treatment suppresses PEDV replication. (A and B) PEDV infection in the presence of CsA. Vero cells were treated with CsA at the indicated concentrations for 1 h prior to infection and were then infected with PEDV (MOI of 0.1). PEDV-infected cells were further maintained for 48 h in the presence of vehicle or CsA. PEDV-specific CPEs were observed daily and were photographed at 48 hpi using an inverted microscope at a magnification of 200 × (first panels). For immunostaining, infected cells were fixed at 48 hpi and stained with anti-PEDV N antibody followed by Alexa green-conjugated goat anti-mouse secondary antibody (second panels). The cells were then counterstained with DAPI (third panels) and examined using a fluorescent microscope at 200 × magnification. Viral production in the presence of CsA was measured by quantifying the number of cells expressing N proteins through IFA. Five fields at 200 × magnification were counted per each condition, and the total number of cells per field as determined by DAPI staining was similar in all fields. Values are representative of the mean of three independent experiments and error bars represent standard deviations. (C) Release of viral progeny in the presence of CsA. Vero cells were pretreated with DMSO or CsA for 1 h and were mock- or PEDV-infected (MOI of 0.1). At 48 hpi, the virus supernatants were collected and viral titers were determined. (D) Growth kinetics of PEDV upon CsA treatment. At the indicated time points after infection, culture supernatants were harvested and viral titers were measured. Results are expressed as the mean values from three independent experiments and error bars represent standard deviations. †, $P < 0.001$.

to infection, and the drug was allowed to remain during infection and subsequent incubation. At 48 hpi, the level of PEDV replication was measured indirectly, as viral antigen production, by quantifying cells expressing the N protein through IFA (Fig. 11A). Treatment of cells with 5 μM *N*-PhMI resulted in a >90% decrease in PEDV production compared to the untreated vehicle control. To further examine the inhibitory effect of *N*-PhMI on PEDV infection, virus production was measured using viral supernatants propagated for 48 h under each condition. As shown in Fig. 11B, inhibition of AIF by *N*-PhMI markedly decreased the titer of PEDV in a dose-dependent manner, and the lowest viral titer was determined to be $10^{2.61}$ PFU/ml at the concentration of 5 μM (an almost 4-log reduction compared to the control). Furthermore, the replication process of PEDV severely interfered with the presence of *N*-PhMI (Fig. 11C). Taken together, our data show that AIF is an essential host determinant in a caspase-independent apoptosis process activated by PEDV, which is indispensable for PEDV replication.

## Discussion

Apoptosis is a tightly controlled multistep process of cell death that occurs in response to a wide range of stimuli, including viral infections. Viruses possess various mechanisms to inhibit apoptosis that allow them to evade the innate immune defenses, which restrict viral infection by eliminating infected cells through the interactions at different stages of the apoptotic pathway. However, some viruses induce apoptosis to facilitate the release and dissemination of viral progeny for further invasion, which are important biological parts in viral pathogenesis and disease processes that promote cell death and tissue injury. Although various viruses are known to modulate apoptosis as a critical armament to complete their replication cycle, it remains so far even undetermined whether PEDV induces apoptosis. In the present study, we characterized PEDV-induced cytotoxicity and demonstrated that apoptotic cell death is triggered in

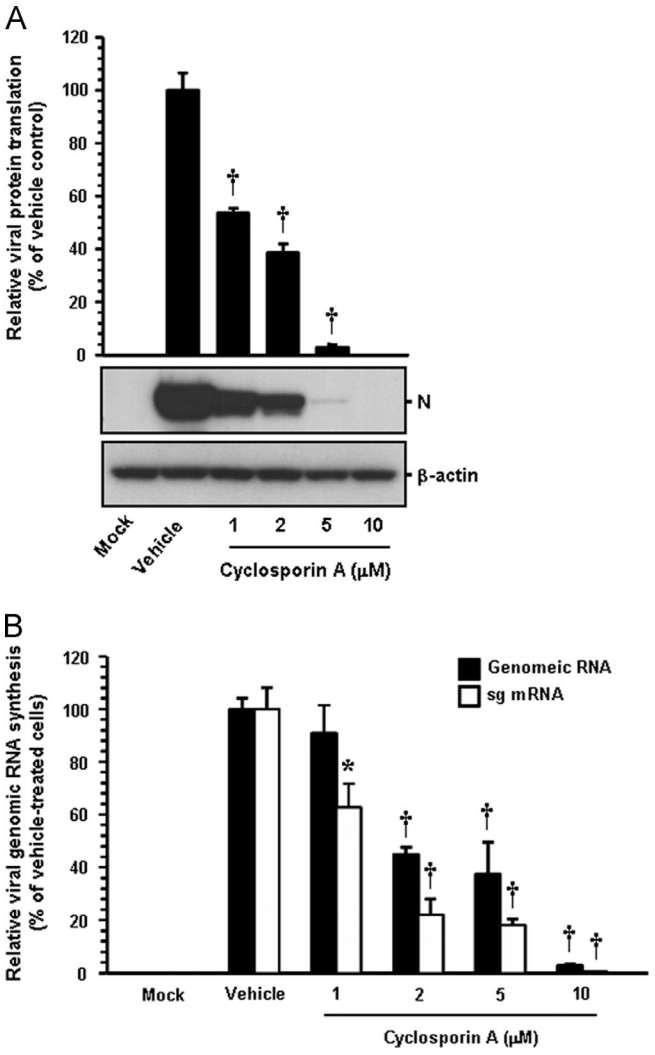


**Fig. 7.** CsA impairs viral protein translation and viral RNA transcription. CsA-treated Vero cells were mock-infected or infected with PEDV (MOI of 0.1) for 1 h and further cultivated in the presence or absence of CsA. (A) At 48 hpi, cellular lysates were prepared, resolved by SDS-PAGE, transferred to a nitrocellulose membrane, and immunoblotted using an antibody against the PEDV N protein. The blot was also reacted with anti-β-actin antibody to verify equal protein loading. PEDV N protein expression was quantitatively analyzed by densitometry in terms of the relative density value to the β-actin gene, and CsA-treated sample results were compared to DMSO-control results. (B) Total cellular RNA was extracted at 48 hpi, and strand-specific viral genomic RNAs (black bars) and sg mRNAs (white bars) of PEDV were amplified by quantitative real-time RT-PCR. Viral positive-sense genomic RNA and sg mRNA levels were normalized to monkey GAPDH mRNA, and relative quantities (RQ) of mRNA accumulation were evaluated. CsA-treated sample results were compared with DMSO-treated results. Values are representative of the mean from three independent experiments and error bars denote standard deviations. *, $P=0.001$ to 0.05; †, $P<0.001$.

PEDV-infected cells *in vitro*, displaying biochemical features of apoptosis including oligonucleosomal DNA fragmentation and PS exposure. This finding strongly suggests that the cytopathology of PEDV infection, represented by vacuolation and syncytia formation *in vitro*, is associated with the apoptotic process. The capability of PEDV to induce apoptosis was also verified by an *in vivo* study using the small intestinal tissues of piglets experimentally inoculated with virulent PEDV. The results showed that the great part of the villus enterocytes in all segments of the small intestine infected with PEDV experienced apoptotic cell death at 3 dpi, and thereafter, cells undergoing apoptosis were more evident inside the small intestine (Fig. 2). Since a specific hallmark of PEDV infection in neonatal piglets is the severe destruction of the villi in the small intestine causing lethal diarrhea and dehydration, PEDV-induced massive apoptosis *in vivo* appears to be one of the viral pathogenic mechanisms to destroy the target enterocytes leading to villus atrophy or vacuolation.

The morphological characteristics of apoptosis are typically caused by the sequential activation of caspases, which are normally present in mammalian cells as inactive precursors (Clarke and Tyler, 2009). Upstream initiator caspases are first activated by both extrinsic and intrinsic apoptotic pathways and subsequently, are responsible for processing and activation of downstream corresponding effector caspases to mediate apoptosis (Clarke and Tyler, 2009; Galluzzi et al., 2012). To understand the molecular mechanisms underlying apoptosis caused by PEDV, we focused on the potential involvement of caspases in apoptotic cell death upon PEDV infection. In the present study, caspase-3, the primary effector caspase, was not proteolytically cleaved to trigger the execution phase of apoptosis during the course of PEDV infection, although its inactive precursor was continuously present in cells infected with PEDV. However, our western blot data, after long exposure, showed only slight levels of caspase-3 activation at 48 hpi (Fig. 3B, second panel). This observation ruled out the possibility that the absence of active caspase-3 was caused by problems with the antibody used or by technical issues. Likewise, chemical suppression of caspase activation was found to be absolutely incapable of abrogating PEDV-induced apoptosis and viral replication. These results strongly indicate that the failure of the pan-caspase inhibitor to protect cell survival is likely a consequence of caspase-independent cell death, which is indispensable for the replication of PEDV.

Our data here reveal that caspases are irrespective of both PEDV-induced apoptosis and viral replication. Thus, we sought to investigate other pro-apoptotic factors that could be involved in PEDV-induced apoptosis, independent of caspases. In response to various intracellular stress conditions, both pro- and anti-apoptotic signals converge toward a mitochondrion-centered control mechanism to trigger intrinsic apoptosis. Under this circumstance, mitochondrial outer membrane permeabilization (MOMP) can begin directly at the outer mitochondrial membrane due to the pore-forming activity of the pro-apoptotic Bax subfamily that translocate from the cytoplasm to the mitochondria or can result from the mitochondrial permeability transition at the inner mitochondria membrane caused by the opening of the mPTP (Brenner and Grimm, 2006; Galluzzi et al., 2012; Tait and Green, 2013). This phenomenon permits the release of several proteins normally retained within the mitochondrial intermembrane space to the cytosol (Galluzzi et al., 2012). Among these, cytosolic CytC participates with other pro-apoptotic factors in the formation of the apoptosome, which triggers the caspase-dependent proteolytic cascade (Galluzzi et al., 2012; Li et al., 1997), whereas AIF, a ubiquitously expressed flavoprotein, critically functions in caspase-independent apoptosis by relocating to the nucleus and promoting large-scale DNA fragmentation and cell death (Galluzzi et al., 2012; Joza et al., 2001; Susin et al., 1999). We demonstrate here that the translocation of mitochondrial AIF to the nucleus was actively manifested during PEDV infection. Conversely, displacement of CytC from the mitochondria to the cytoplasm was completely absent in PEDV-infected cells. This result further supports the hypothesis that PEDV triggers apoptosis in a caspase-independent manner. The association of PEDV-induced apoptosis with AIF translocation to the cytosol, without the release of CytC followed by caspase activation, indicates that AIF is the sole pro-apoptotic factor released via altered mitochondrial membrane permeability and primarily acts directly to execute apoptotic cell death in PEDV infection.

The unique relocation of AIF, but not CytC, leads us to speculate that MOMP may be regulated by the opening process following

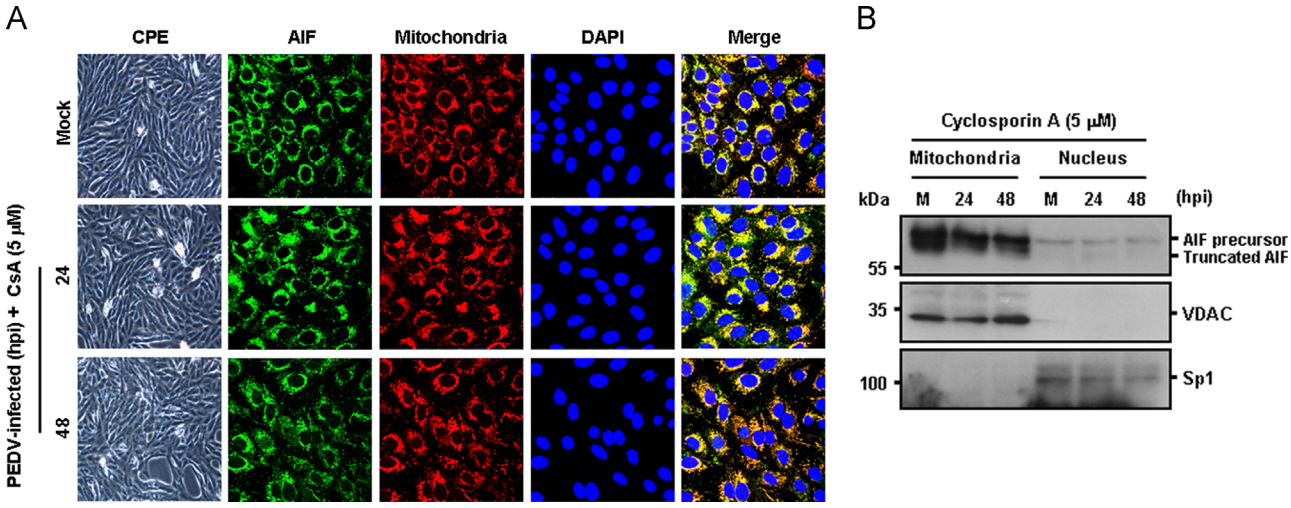


**Fig. 8.** CsA treatment blocks AIF nuclear translocation. (A) Immunofluorescent detection of AIF in the presence of CsA. Vero cells were preincubated with CsA (5 μM) for 1 h and were mock-infected or infected with PEDV (MOI of 0.1). At 24 hpi and 48 hpi, cells were labeled with MitoTracker Red CMXRos (red), fixed, and incubated with an anti-AIF antibody (green). AIF mitochondrial colocalization is represented by merged AIF and the mitochondrial marker (yellow). (B) Western blot analysis of AIF in the presence of CsA. Each mitochondrial and nuclear fraction was prepared under the indicated conditions and subjected to western blotting with an antibody against AIF (top panel), VDAC as a mitochondrial protein marker (middle panel), or Sp1 as a nuclear protein marker (bottom panel). Lane M, mock-infected.

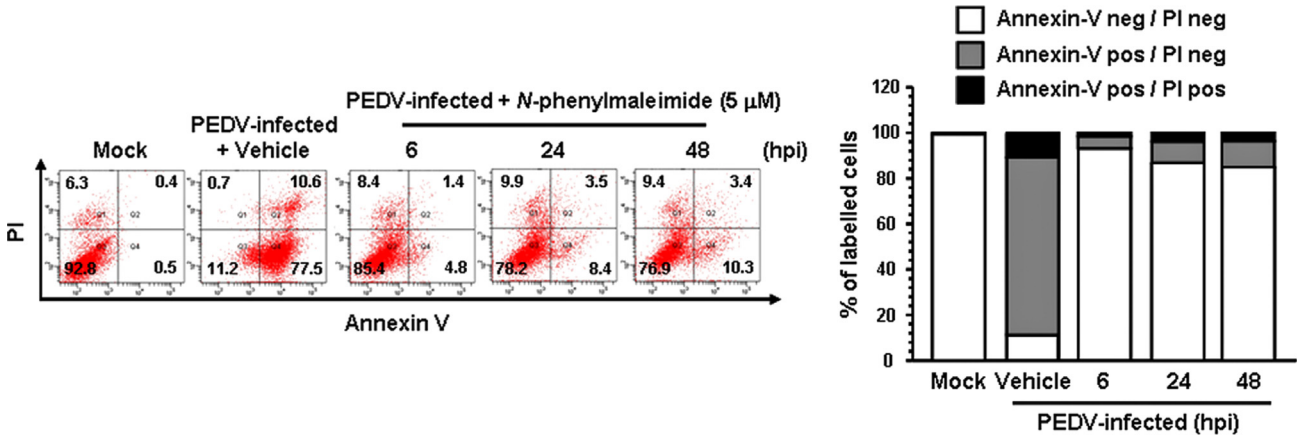


**Fig. 9.** *N*-PhMI treatment diminishes PEDV-induced apoptosis. Vero cells were treated with *N*-PhMI (5 μM) or DMSO for 1 h prior to infection and then mock-infected or infected with PEDV in the presence of vehicle or *N*-PhMI. Cells were harvested at the indicated time points, dually labeled with Annexin V and PI, and subjected to FACS analysis. The bottom graph represents the percentage of each quadrant.

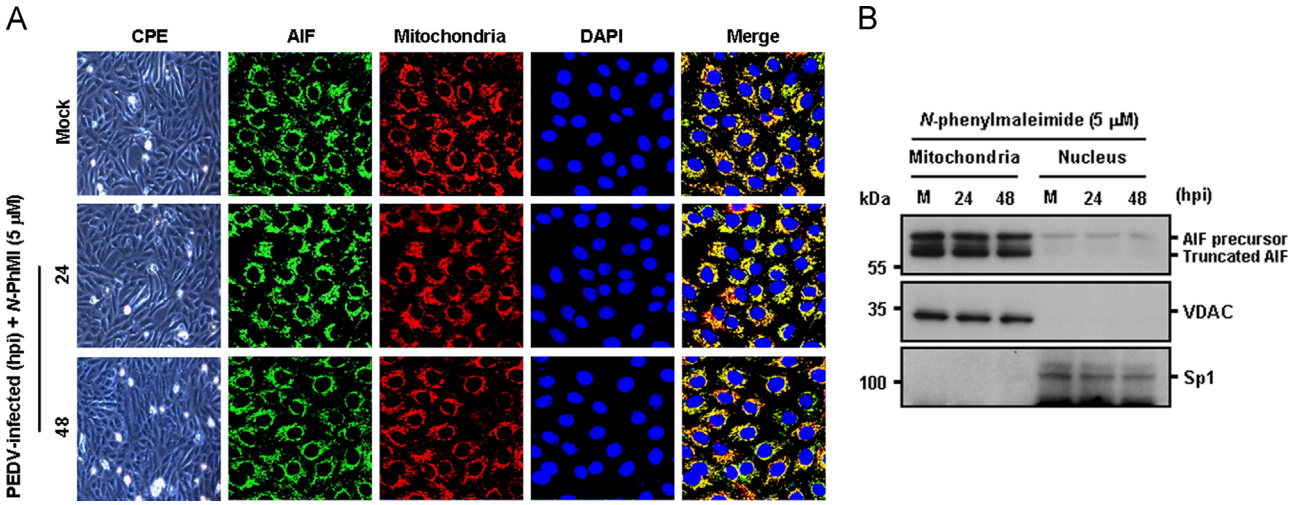


**Fig. 10.** *N*-PhMI treatment hampers AIF nuclear translocation. (A) Immunofluorescent detection of AIF in the presence of *N*-PhMI. Vero cells were pretreated with *N*-PhMI CsA for 1 h and were mock-infected or infected with PEDV (MOI of 0.1). At 24 hpi and 48 hpi, cells were labeled with MitoTracker Red CMXRos (red), fixed, and incubated with an anti-AIF antibody (green). AIF mitochondrial accumulation is indicated by merged AIF and the mitochondrial marker (yellow). (B) Western blot analysis of AIF in the presence of *N*-PhMI. Each mitochondrial and nuclear fraction was prepared under the indicated conditions and subjected to western blotting with an antibody against AIF (top panel), VDAC as a mitochondrial protein marker (middle panel), or Sp1 as a nuclear protein marker (bottom panel). Lane M, mock-infected.

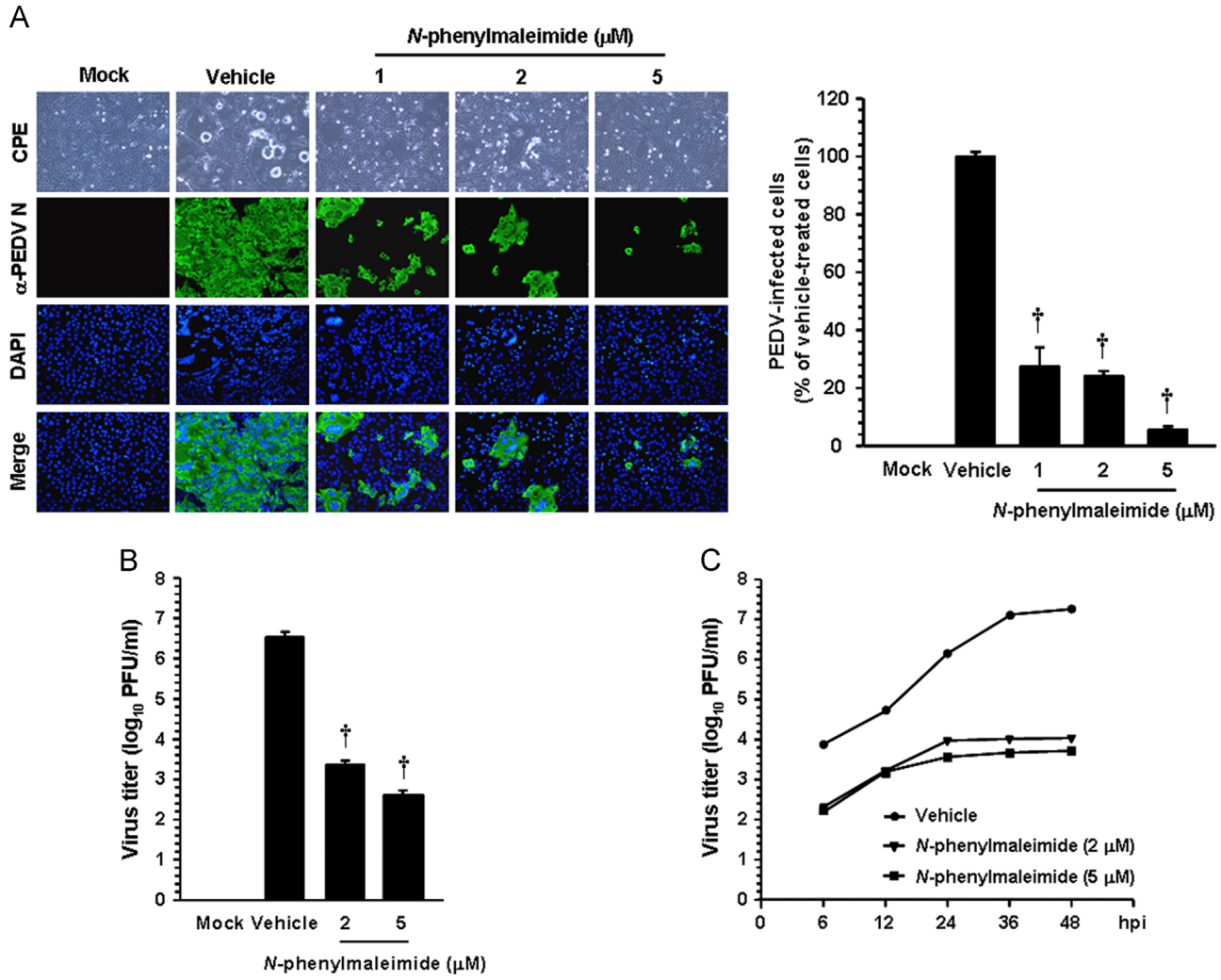


**Fig. 11.** *N*-PhMI treatment inhibits PEDV infection. (A) PEDV propagation in the presence of CsA. Vero cells were pretreated with *N*-PhMI at the indicated concentrations for 1 h and then infected with PEDV (MOI of 0.1). PEDV-infected cells were further maintained for 48 h in the presence of a vehicle or *N*-PhMI. PEDV-specific CPEs were observed daily and were photographed at 48 hpi using an inverted microscope at a magnification of 200 × (first panels). At 48 hpi, virus-infected cells were subjected to IFA with anti-PEDV N antibody (second panels) followed by DAPI counterstaining (third panels) and examined using a fluorescent microscope at 200 × magnification. Viral production in the presence of *N*-PhMI was assessed exactly as described in the legend to Fig. 6B. (B) Progeny virus release in the presence of *N*-PhMI. Vero cells were pretreated with DMSO or *N*-PhMI for 1 h and were mock- or PEDV-infected (MOI of 0.1). At 48 hpi, the virus supernatants were collected and viral titers were measured. (C) Growth kinetics of PEDV upon *N*-PhMI treatment. At the indicated time points post-infection, culture supernatants were harvested and viral titers were determined. Results are expressed as the mean values from three independent experiments and error bars represent standard deviations. †, $P < 0.001$.

mPTP formation during PEDV infection, in which CypD functions as a major inducing factor to constitute the mPTP complex in the mitochondrial membrane. The data clearly show that inhibition of CypD by CsA blocked apoptosis induced by PEDV and was accompanied by 70–80% cell survival after PEDV infection, comparable to mock-infected cells. Furthermore, CsA could exert the antiviral activity via potent inhibition of multiple steps of the PEDV life cycle, including viral translation, RNA synthesis, and spread of viral progeny. Notably, chemical suppression of CypD impaired AIF nuclear translocation, leading to absolute mitochondrial retention of AIF. Thus, CypD-mediated mPTP modulation plays a pivotal role in caspase-independent apoptotic cell death by controlling AIF translocation upon PEDV infection. Numerous putative cellular proteins are known to bind with CypD to promote mPTP formation. Bax is one such factor, which has been shown to be displaced toward the mitochondria and to interact subsequently with CypD to facilitate the formation of pores in the mitochondrial membrane in response to apoptotic stimuli, including viral infection (Favreau et al., 2012; Kumarswamy and Chandna, 2009). Although it is unclear whether Bax is directly involved in PEDV-induced apoptosis, this mechanism is less plausible because PEDV infection was irrelevant to mitochondrial CytC release, which is mainly mediated by mitochondrial translocation of Bax. Similarly, direct inhibition of AIF with a chemical inhibitor completely confined AIF protein in the mitochondria without nuclear localization, and robustly diminished PEDV-induced apoptotic cell death and PEDV replication. The inhibitory activity of *N*-PhMI on PEDV infection was less efficient than that of CsA, although treatment with *N*-PhMI also exhibited significant suppression of PEDV replication in its own way. This difference can be attributed to the wide-spectrum antiviral effect of CsA via multiple simultaneous mechanisms; CsA is known to inhibit the replication of several RNA viruses, including nidoviruses, by affecting the function of various members of the cellular cyclophilin protein family (de Wilde et al., 2013; Kambara et al., 2011; Nakagawa et al., 2004; Pfefferle et al., 2011; Qing et al., 2009;). Moreover, it was recently demonstrated that CsA fully blocks arterivirus replication by suppressing viral RNA synthesis (Wilde et al., 2013). We also showed here that treatment of cells with CsA dramatically reduces synthesis of both genomic RNA and sg mRNA

(Fig. 7B). Therefore, CsA appears to synergistically elicit its antiviral activity on the replication of PEDV through inhibition of apoptotic cell death and interference with viral RNA synthesis.

In summary, our findings described here reveal that PEDV induces apoptotic cell death, which represents a cytolytic mechanism causing CPEs *in vitro* and contributes to PEDV pathogenicity by damaging the villous enterocytes of the small intestine, leading to malabsorptive diarrhea. However, PEDV-induced apoptosis was neither inhibited by Z-VAD-FMK nor accompanied by the activation of caspase cascades and the concomitant release of CytC from the mitochondria, strongly indicating that this cell death event by PEDV is caspase-dispensable. On the other hand, we demonstrated the essential roles of CypD and AIF in PEDV-induced apoptosis; in response to PEDV infection, MOMP occurs through opening of the mPTP dependent on CypD, which collapses the mitochondrial potential, resulting in the characteristic release of AIF to the nucleus and thereby mediating large-scale DNA fragmentation. Furthermore, inhibition of either CypD or AIF robustly abrogated the life cycle of PEDV at subcytotoxic doses. To our knowledge, this is the first report of CypD-involved, AIF-indispensable apoptosis, independent of both caspase activation and CytC release following viral infection. Although mitochondrial CypD and AIF necessarily contribute to PEDV-induced apoptosis, the upstream intracellular regulatory signal(s) and the viral protein(s) that are associated with this mitochondrion-centered apoptotic pathway mediated by PEDV infection are still unclear and accordingly, identification of such cellular and viral factors would be the next issue to be addressed in future studies. In conclusion, the results presented here indicate that PEDV induces apoptotic cell death via a caspase-independent, AIF-mediated pathway that plays a critical role in PEDV replication and pathogenesis and suggest that the anti-apoptotic approach may be one of appropriate strategies for the development of an anti-PEDV compound to combat PED.

## Material and methods

### *Cells, viruses, reagents, and antibodies*

Vero cells were cultured in alpha minimum essential medium (α-MEM; Invitrogen) with 10% fetal bovine serum (FBS; Invitrogen) and antibiotic-antimycotic solutions (100 × ; Invitrogen). The cells were maintained at 37 °C in a humidified 5% $CO_2$ incubator. PEDV strain SM98-1 was kindly provided by the Korean Animal and Plant Quarantine Agency and propagated in Vero cells as described previously (Hofmann and Wyler, 1988). Staurosporine was purchased from Cayman Chemical Company and used at a concentration of 1 μg/ml to induce apoptosis. Z-VAD-FMK (R&D Systems), cyclosporin A (CsA; Cell Signaling Technologies), and *N*-phenylmaleimide (*N*-PhMI; Sigma-Aldrich) were dissolved in dimethyl sulfoxide (DMSO) to yield a 20 mM, 10 mM, or 1 M stock, respectively. The PEDV N protein-specific monoclonal antibody (MAb) was a kind gift from Sang-Geon Yeo (Kyungpook National University, Daegu, Korea). Antibodies specific for AIF, CytC, Sp1, and β-actin and horseradish peroxidase (HRP)-conjugated secondary antibodies were obtained from Santa Cruz Biotechnology. The caspase-3, voltage-dependent anion channel (VDAC), and α-tubulin antibodies were purchased from Sigma-Aldrich.

### *Cell viability assay*

The cytotoxic effects of reagents on Vero cells were analyzed using a colorimetric 3-(4,5-dimethylthiazol-2-yl)-2,5-diphenyltetrazolium bromide (MTT) assay (Sigma-Aldrich) to detect cell viability. Briefly, Vero cells were grown at $1 \times 10^4$ cells/well in a 96-well tissue culture plate with Z-VAD-FMK, CsA or *N*-PhMI treatment for 24 h. After 1 day of incubation, 50 μl of MTT solution (1.1 mg/ml) was added to each well, and the samples were incubated for an additional 4 h. The supernatant was then removed from each well, after which 150 μl of DMSO was added to dissolve the colored formazan crystals produced by the MTT. The absorbance of the solution was measured at 540 nm using an enzyme-linked immunosorbent assay plate reader. All MTT assays were performed in triplicate.

### *DNA fragmentation assay*

Vero cells were grown at $3.5 \times 10^5$ cells/well in 6-well tissue culture plates for 1 day and then mock infected or infected with PEDV at a multiplicity of infection (MOI) of 0.1. In addition, cells were pretreated with Z-VAD-FMK or CsA for 1 h followed by PEDV infection. At the indicated times, cells were harvested, washed with PBS, and then incubated in a cell lysis buffer (10 mM Tris, pH 7.5, 1 mM EDTA, and 0.2% Triton X-100) containing 500 μg/ml protease K for 24 h at 55 °C. The DNA was then extracted twice with phenol/chloroform, precipitated with isopropanol, and resuspended in distilled water. Next, the purified DNA was incubated with 20 μg/ml ribonuclease A for 1 h at 37 °C, electrophoresed on a 1.2% agarose gel containing Midori Green Advanced DNA Stain (NIPPON Genetics), and photographed.

### *Annexin V and PI staining assay*

Vero cells were grown in 6-well tissue culture plates for 1 day and mock infected or infected with PEDV at an MOI of 0.1. To examine the effect of each inhibitor on PEDV-induced apoptosis, cells were treated with Z-VAD-FMK, CsA, or *N*-PhMI and then infected with PEDV. The virus-inoculated cells were further propagated in the presence of Z-VAD-FMK (100 μM), CsA (5 μM), *N*-PhMI (5 μM) or DMSO (vehicle control). Phosphatidylserine exposure was determined by measuring Annexin V binding at the indicated times using an Alexa Fluor 488 Annexin V/Dead Cell Apoptosis kit (Invitrogen), according to the manufacturer's protocol. In brief, cells were harvested, washed with cold PBS, and suspended in 100 μl 1 × annexin-binding buffer. The cells were then incubated with Alexa Fluor 488-conjugated Annexin V and propidium iodide (PI) at room temperature (RT) for 15 min in the dark. Following the incubation period, 400 μl of annexin-binding buffer was added to each sample, and the samples were mixed gently and kept on ice. The fluorescent signals of Annexin V and PI were detected at channels FL-1 and FL-2, respectively, and analyzed using a fluorescence-activated cell sorter (FACS) Aria III flow cytometer (BD Biosciences). Cells negative for PI uptake and positive for Annexin V were considered apoptotic.

### *TUNEL labeling assay*

Vero cells were grown on microscope coverslips placed in 6-well tissue culture plates and mock infected or infected with PEDV at a MOI of 0.1. The virus-infected cells were fixed at 48 h post-infection (hpi) with 4% paraformaldehyde for 25 min at 4 °C and permeabilized with 0.2% Triton X-100 in PBS at RT for 5 min. For tissue labeling, two 4 day-old piglets were orally inoculated with 1 ml of small intestine homogenate containing $10^5$ $TCID_{50}$ of a PEDV field isolate as described previously (Oh et al., in press), and tissue specimens were collected from the duodenum, jejunum, and ileum of piglets at 3 and 5 days post-inoculation (dpi) at necropsy. Each small intestinal tissue ( < 3 mm thick) was fixed with 10% formalin for 24 h at RT and embedded in paraffin according to standard laboratory procedures. The formalin-fixed, paraffin-embedded tissues were cut to slices 5–8 μm thick on a microtome, floated on a 40 °C water bath containing distilled

water, and transferred onto glass slides. The tissues were then deparaffinized in xylene for 5 min and washed in decreasing concentrations of ethanol (100%, 95%, 85%, 70%, and 50%), for 3 min each. The sections were fixed with 4% paraformaldehyde for 15 min, permeabilized with 20 μg/ml proteinase K solution at RT for 10 min, and fixed again with 4% paraformaldehyde for 5 min. A terminal deoxynucleotidyl transferase-catalyzed deoxyuridine phosphate-nick end labeling (TUNEL) assay was performed using a DeadEnd Fluorometric TUNEL System kit (Promega) according to the manufacturer's instructions with some modifications. Briefly, PEDV-infected Vero cells and the deparaffinized intestinal tissue sections were rinsed twice with PBS, and the TUNEL reaction mixture was added, incubated for 60 min at 37 °C, immersed in 2 × SSC buffer for 15 min, and washed 3 times in PBS. TUNEL-labeled cells were subjected to an immunofluorescence assay using N-specific MAb and Alexa Fluor 594-conjugated goat anti-mouse antibody as described below. The samples were mounted on microscope glass slides in mounting buffer (60% glycerol and 0.1% sodium azide in PBS) and analyzed under a Confocal Laser Scanning microscope (Carl Zeiss) using an excitation wavelength in the range of 450–500 nm and an emission wavelength in the range of 515–565 nm.

*Immunofluorescence assay (IFA)*

Vero cells grown on microscope coverslips placed in 6-well tissue culture plates were pretreated with Z-VAD-FMK, CsA or *N*-PhMI for 1 h and mock infected or infected with PEDV at a MOI of 0.1. The virus-infected cells were subsequently grown in the presence of inhibitors until 48 hpi, fixed with 4% paraformaldehyde for 10 min at RT and permeabilized with 0.2% Triton X-100 in PBS at RT for 10 min. The cells were blocked with 1% bovine serum albumin (BSA) in PBS for 30 min at RT and then incubated with N-specific MAb for 2 h. After being washed five times in PBS, the cells were incubated for 1 h at RT with a goat anti-mouse secondary antibody conjugated to Alexa Fluor 488 (Invitrogen), followed by counterstaining with 4′,6-diamidino-2-phenylindole (DAPI; Sigma-Aldrich). The coverslips were mounted on microscope glass slides in mounting buffer and cell staining was visualized using a fluorescent Leica DM IL LED microscope (Leica). For study of colocalization, MitoTracker Red CMXRos (200 nM; Invitrogen) was added to viable Vero cells and left for 45 min at 37 °C prior to fixation. The cells were then stained with AIF- or CytC-specific antibody as described above, and cell staining was analyzed using a Confocal Laser Scanning microscope (Carl Zeiss).

*Cell fractionation and western blot analysis*

Vero cells were grown in 6-well tissue culture plates for 1 day and were mock infected or infected with PEDV at an MOI of 0.1. At the indicated times, cells were harvested in 50 μl of lysis buffer (0.5% TritonX-100, 60 mM β-glycerophosphate, 15 mM ρ-nitro phenyl phosphate, 25 mM MOPS, 15 mM, $MgCl_2$, 80 mM NaCl, 15 mM EGTA [pH 7.4], 1 mM sodium orthovanadate, 1 μg/ml E64, 2 μg/ml aprotinin, 1 μg/ml leupeptin, and 1 mM PMSF) and sonicated on ice 5 times for 1 s each. Homogenates were lysed for 30 min on ice, and clarified by centrifugation at 15,800 × × × *g* (Eppendorf centrifuge 5415R) for 30 min at 4 °C. For cell fractionation, inhibitor-treated, PEDV-infected Vero cells were fractionated using a Nuclear/Cytosol or Mitochondria/Cytosol Fractionation Kit (BioVision) according to the manufacturer's manuals. The total protein concentrations in the supernatants were determined using a BCA protein assay (Pierce). Equal amounts of total protein were separated on a NuPAGE 4–12% gradient Bis-Tris gel (Invitrogen) under reducing conditions and electrotransferred onto Immunobilon-P (Millipore). The membranes were subsequently blocked with 3% powdered skim milk (BD Biosciences) in TBS (10 mM Tris–HCl [pH 8.0], 150 mM NaCl) with 0.05% Tween-20 (TBST) at 4 °C for 2 h and incubated at 4 °C overnight with the primary antibodies. The blots were then incubated with corresponding secondary HRP-labeled antibodies at a dilution of 1:5000 for 2 h at 4 °C. Proteins were visualized using enhanced chemiluminescence (ECL) reagents (GE Healthcare) according to the manufacturer′s instructions. To quantify viral protein production, band densities of PEDV N proteins were quantitatively analyzed using a computer densitometer with the Wright Cell Imaging Facility (WCIF) version of the ImageJ software package (http://www.uhnresearch.*ca*/facilities/wcif/imagej/) based on the density value relative to the β-actin protein.

*Virus titration*

Vero cells were PEDV infected and treated with Z-VAD-FMK, CsA, *N*-PhMI or DMSO as described above. The culture supernatant was collected at different time points (6, 12, 24, 36, and 48 hpi) and stored at −80 °C. The PEDV titer was determined by a plaque assay using Vero cells and quantified as plaque-forming units (PFU) per ml.

*Quantitative real-time RT-PCR*

Vero cells were PEDV inoculated with treatment of CsA for 1 h at 37 °C. The virus inoculum was subsequently removed and the infected cells were maintained in fresh medium containing CsA for 48 h. Total RNA was extracted from lysates of the infected cells at 48 hpi using TRIzol reagent (Invitrogen) and treated with DNase I (TaKaRa) according to the manufacturer′s protocols. The concentrations of the extracted RNA were measured using a NanoVue spectrophotometer (GE Healthcare). Quantitative real-time RT-PCR was conducted using a Thermal Cycler Dice Real Time System (TaKaRa) with gene-specific primer sets described previously (Kim and Lee, 2013). The RNA levels of viral genes were normalized to that of mRNA for the glyceraldehyde-3-phosphate dehydrogenase (GAPDH) gene, and relative quantities (RQ) of mRNA accumulation were evaluated using the $2^{-\Delta\Delta Ct}$ method. To detect alteration of genomic RNA and subgenomic (sg) mRNA levels in the presence of CsA during PEDV infection, the results obtained using CsA-treated samples were compared with vehicle-treated results.

*Statistical analysis*

All statistical analyses were performed using Student′s *t*-test, and *P*-values of less than 0.05 were considered statistically significant.

## Acknowledgment

This research was supported by Basic Science Research Program through the National Research Foundation of Korea (NRF) funded by the Korean Ministry of Education, Science and Technology (NRF-2012R1A1A2039746).

## Appendix A. Supporting information

Supplementary data associated with this article can be found in the online version at http://dx.doi.org/10.1016/j.virol.2014.04.040.

## References

Baines, C.P., Kaiser, R.A., Purcell, N.H., Blair, N.S., Osinska, H., Hambleton, M.A., Brunskill, E.W., Sayen, M.R., Gottlieb, R.A., Dorn, G.W., Robbins, J., Molkentin, J.

D., 2005. Loss of cyclophilin D reveals a critical role for mitochondrial permeability transition in cell death. Nature 434, 658–662.
Brenner, C., Grimm, S., 2006. The permeability transition pore complex in cancer cell death. Oncogene 25, 4744–4756.
Chen, J.F., Sun, D.B., Wang, C.B., Shi, H.Y., Cui, X.C., Liu, S.W., Qiu, H.J., Feng, L., 2008. Molecular characterization and phylogenetic analysis of membrane protein genes of porcine epidemic diarrhea virus isolates in China. Virus Genes 36, 355–364.
Clarke, P., Beckham, J.D., Leser, J.S., Hoyt, C.C., Tyler, K.L., 2009. Fas-mediated apoptotic signaling in the mouse brain following reovirus infection. J. Virol. 83, 6161–6170.
Clarke, P., Tyler, K.L., 2009. Apoptosis in animal models of virus-induced disease. Nat. Rev. Microbiol. 7, 144–155.
Cregan, S.P., Fortin, A., MacLaurin, J.G., Callaghan, S.M., Cecconi, F., Yu, S.W., Dawson, T.M., Dawson, V.L., Park, D.S., Kroemer, G., Slack, R.S., 2002. Apoptosis-inducing factor is involved in the regulation of caspase-independent neuronal cell death. J. Cell Biol. 158, 507–517.
Daugas, E., Nochy, D., Ravagnan, L., Loeffler, M., Susin, S.A., Zamzami, N., Kroemer, G., 2000. Apoptosis-inducing factor (AIF): a ubiquitous mitochondrial oxidoreductase involved in apoptosis. FEBS Lett. 476, 118–123.
Debouck, P., Pensaert, M., 1980. Experimental infection of pigs with a new porcine enteric coronavirus, CV 777. Am. J. Vet. Res. 41, 219–223.
DeDiego, M.L., Nieto-Torres, J.L., Jiménez-Guardeño, J.M., Regla-Nava, J.A., Alvarez, E., Oliveros, J.C., Zhao, J., Fett, C., Perlman, S., Enjuanes, L., 2011. Severe acute respiratory syndrome coronavirus envelope protein regulates cell stress response and apoptosis. PLoS Pathog. 7, e1002315.
de Wilde, A.H., Li, Y., van der Meer, Y., Vuagniaux, G., Lysek, R., Fang, Y., Snijder, E.J., van Hemert, M.J., 2013. Cyclophilin inhibitors block arterivirus replication by interfering with viral RNA synthesis. J. Virol. 87, 1454–1464.
Duarte, M., Tobler, K., Bridgen, A., Rasschaert, D., Ackermann, M., Laude, H., 1994. Sequence analysis of the porcine epidemic diarrhea virus genome between the nucleocapsid and spike protein genes reveals a polymorphic ORF. Virology 198, 466–476.
Eleouet, J.F., Chilmonczyk, S., Besnardeau, L., Laude, H., 1998. Transmissible gastroenteritis coronavirus induces programmed cell death in infected cells through a caspase-dependent pathway. J. Virol. 72, 4918–4924.
Favreau, D.J., Meessen-Pinard, M., Desforges, M., Talbot, P.J., 2012. Human coronavirus-induced neuronal programmed cell death is cyclophilin d dependent and potentially caspase dispensable. J. Virol. 86, 81–93.
Galluzzi, L., Kepp, O., Trojel-Hansen, C., Kroemer, G., 2012. Mitochondrial control of cellular life, stress, and death. Circ. Res. 111, 1198–1207.
Hofmann, M., Wyler, R., 1988. Propagation of the virus of porcine epidemic diarrhea in cell culture. J. Clin. Microbiol. 26, 2235–2239.
Joza, N., Susin, S.A., Daugas, E., Stanford, W.L., Cho, S.K., Li, C.Y., Sasaki, T., Elia, A.J., Cheng, H.Y., Ravagnan, L., Ferri, K.F., Zamzami, N., Wakeham, A., Hakem, R., Yoshida, H., Kong, Y.Y., Mak, T.W., Zúñiga-Pflücker, J.C., Kroemer, G., Penninger, J.M., 2001. Essential role of the mitochondrial apoptosis-inducing factor in programmed cell death. Nature 410, 549–554.
Kambara, H., Tani, H., Mori, Y., Abe, T., Katoh, H., Fukuhara, T., Taguwa, S., Moriishi, K., Matsuura, Y., 2011. Involvement of cyclophilin B in the replication of Japanese encephalitis virus. Virology 412, 211–219.
Kocherhans, R., Bridgen, A., Ackermann, M., Tobler, K., 2001. Completion of the porcine epidemic diarrhoea coronavirus (PEDV) genome sequence. Virus Genes 23, 137–144.
Kroemer, G., Galluzzi, L., Vandenabeele, P., Abrams, J., Alnemri, E.S., Baehrecke, E.H., Blagosklonny, M.V., El-Deiry, W.S., Golstein, P., Green, D.R., Hengartner, M., Knight, R.A., Kumar, S., Lipton, S.A., Malorni, W., Nuñez, G., Peter, M.E., Tschopp, J., Yuan, J., Piacentini, M., Zhivotovsky, B., Melino, G., 2009. Classification of cell death: recommendations of the Nomenclature Committee on Cell Death 2009. Cell Death Differ. 16, 3–11.
Kumarswamy, R., Chandna, S., 2009. Putative partners in Bax mediated cytochrome-c release: ANT, CypD, VDAC or none of them? Mitochondrion 9, 1–8.
Kweon, C.H., Kwon, B.J., Jung, T.S., Kee, Y.J., Hur, D.H., Hwang, E.K., et al., 1993. Isolation of porcine epidemic diarrhea virus (PEDV) in Korea. Korean J. Vet. Res. 33, 249–254.
Kim, Y., Lee, C., 2013. Ribavirin efficiently suppresses porcine nidovirus replication. Virus Res. 171, 44–53.
Lan, Y., Zhao, K., Wang, G., Dong, B., Zhao, J., Tang, B., Lu, H., Gao, W., Chang, L., Jin, Z., Gao, F., He, W., 2013. Porcine hemagglutinating encephalomyelitis virus induces apoptosis in a porcine kidney cell line via caspase-dependent pathways. Virus Res. 176, 292–297.
Lee, S.M., Kleiboeker, S.B., 2007. Porcine reproductive and respiratory syndrome virus induces apoptosis through a mitochondria-mediated pathway. Virology 365, 419–434.
Li, W., Li, H., Liu, Y., Pan, Y., Deng, F., Song, Y., Tang, X., He, Q., 2012. New variants of porcine epidemic diarrhea virus, China, 2011. Emerg. Infect. Dis. 18, 1350–1353.
Li, P., Nijhawan, D., Budihardjo, I., Srinivasula, S.M., Ahmad, M., Alnemri, E.S., Wang, X., 1997. Cytochrome c and dATP-dependent formation of Apaf-1/caspase-9 complex initiates an apoptotic protease cascade. Cell 91, 479–489.
Lu, J.R., Lu, W.W., Lai, J.Z., Tsai, F.L., Wu, S.H., Lin, C.W., Kung, S.H., 2013. Calcium flux and calpain-mediated activation of the apoptosis-inducing factor contribute to enterovirus 71-induced apoptosis. J. Gen. Virol. 94, 1477–1485.
Mole, 2013. Deadly pig virus slips through US borders. Nature 499, 388.
Nakagawa, M., Sakamoto, N., Enomoto, N., Tanabe, Y., Kanazawa, N., Koyama, T., Kurosaki, M., Maekawa, S., Yamashiro, T., Chen, C.H., Itsui, Y., Kakinuma, S., Watanabe, M., 2004. Specific inhibition of hepatitis C virus replication by cyclosporin A. Biochem. Biophys. Res. Commun. 313, 42–47.
Oh, J., Lee, K.-W., Choi, H.-W., Lee, C., 2014. Immunogenicity and efficacy of recombinant S1 domain of the porcine epidemic diarrhea virus spike protein, Arch. Virol., in press.
Oldham J.,1972. Letter to the editor. Pig Farming vol. 10, pp. 72–73.
Pensaert, M.B., de Bouck, P., 1978. A new coronavirus-like particle associated with diarrhea in swine. Arch. Virol. 58, 243–247.
Pensaert, M.B., de Bouck, P., Reynolds, D.J., 1981. An immunoelectron microscopic and immunofluorescent study on the antigenic relationship between the coronavirus-like agent, CV 777, and several coronaviruses. Arch. Virol. 68, 45–52.
Pfefferle, S., Schopf, J., Kogl, M., Friedel, C.C., Müller, M.A., Carbajo-Lozoya, J., Stellberger, T., von Dall'Armi, E., Herzog, P., Kallies, S., Niemeyer, D., Ditt, V., Kuri, T., Züst, R., Pumpor, K., Hilgenfeld, R., Schwarz, F., Zimmer, R., Steffen, I., Weber, F., Thiel, V., Herrler, G., Thiel, H.J., Schwegmann-Wessels, C., Po hlmann, S., Haas, J., Drosten, C., von Brunn, A., 2011. The SARS-coronavirus-host interactome: identification of cyclophilins as target for pan-coronavirus inhibitors. PLoS Pathog. 7, e1002331.
Puranaveja, S., Poolperm, P., Lertwatcharasarakul, P., Kesdaengsakonwut, S., Boonsoongnern, A., Urairong, K., Kitikoon, P., Choojai, P., Kedkovid, R., Teankum, K., Thanawongnuwech, R., 2009. Chinese-like strain of porcine epidemic diarrhea virus, Thailand. Emerg. Infect. Dis. 15, 1112–1115.
Qing, M., Yang, F., Zhang, B., Zou, G., Robida, J.M., Yuan, Z., Tang, H., Shi, P.Y., 2009. Cyclosporine inhibits flavivirus replication through blocking the interaction between host cyclophilins and viral NS5 protein. Antimicrob. Agents Chemother. 53, 3226–3235.
Saif, L.J., Pensaert, M.B., Sestack, K., Yeo, S.G., Jung, K., 2012. Coronaviruses. In: Straw, B.E., Zimmerman, J.J., Karriker, L.A., Ramirez, A., Schwartz, K.J., Stevenson, G.W. (Eds.), Diseases of Swine. Wiley-Blackwell, Ames, IA, pp. 501–524.
Sarmento, L., Tseggai, T., Dhingra, V., Fu, Z.F., 2006. Rabies virus-induced apoptosis involves caspase-dependent and caspase-independent pathways. Virus Res. 121, 144–151.
Schinzel, A.C., Takeuchi, O., Huang, Z., Fisher, J.K., Zhou, Z., Rubens, J., Hetz, C., Danial, N.N., Moskowitz, M.A., Korsmeyer, S.J., 2005. Cyclophilin D is a component of mitochondrial permeability transition and mediates neuronal cell death after focal cerebral ischemia. Proc. Natl. Acad. Sci. USA 102, 12005–12010.
Stevenson, G.W., Hoang, H., Schwartz, K.J., Burrough, E.R., Sun, D., Madson, D., Cooper, V.L., Pillatzki, A., Gauger, P., Schmitt, B.J., Koster, L.G., Killian, M.L., Yoon, K.J., 2013. Emergence of Porcine epidemic diarrhea virus in the United States: clinical signs, lesions, and viral genomic sequences. J. Vet. Diagn. Invest. 25, 649–654.
St-Louis, M.C., Archambault, D., 2007. The equine arteritis virus induces apoptosis via caspase-8 and mitochondria-dependent caspase-9 activation. Virology 367, 147–155.
Susin, S.A., Lorenzo, H.K., Zamzami, N., Marzo, I., Snow, B.E., Brothers, G.M., Mangion, J., Jacotot, E., Costantini, P., Loeffler, M., Larochette, N., Goodlett, D. R., Aebersold, R., Siderovski, D.P., Penninger, J.M., Kroemer, G., 1999. Molecular characterization of mitochondrial apoptosis-inducing factor. Nature 397, 441–446.
Susin, S.A., Zamzami, N., Castedo, M., Hirsch, T., Marchetti, P., Macho, A., Daugas, E., Geuskens, M., Kroemer, G., 1996. Bcl-2 inhibits the mitochondrial release of an apoptogenic protease. J. Exp. Med. 184, 1331–1341.
Suzuki, K., Matsui, Y., Miura, Y., Sentsui, H., 2008. Equine coronavirus induces apoptosis in cultured cells. Vet. Microbiol. 129, 390–395.
Tait, S.W., Green, D.R., 2013. Mitochondrial regulation of cell death. Cold Spring Harbor Perspect. Biol. 5, a008706.
Takahashi, K., Okada, K., Ohshima, K., 1983. An outbreak of swine diarrhea of a new-type associated with coronavirus-like particles in Japan. Jpn. J. Vet. Sci. 45, 829–832.
Thomson, B.J., 2001. Viruses and apoptosis. Int. J. Exp. Pathol. 82, 65–76.
Wang, M.J., Liu, S., Liu, Y., Zheng, D., 2007. Actinomycin D enhances TRAIL-induced caspase-dependent and -independent apoptosis in SH-SY5Y neuroblastoma cells. Neurosci. Res. 59, 40–46.
Yuste, V.J., Moubarak, R.S., Delettre, C., Bras, M., Sancho, P., Robert, N., d'Alayer, J., Susin, S.A., 2005. Cysteine protease inhibition prevents mitochondrial apoptosis-inducing factor (AIF) release. Cell Death Differ. 12, 1445–1448.